μFLU12-108

STREAMING POTENTIAL OF AN ELECTROLYTE IN A MICROCHANNEL WITH A LATERAL TEMPERATURE GRADIENT

Mathias Dietzel*, **Steffen Hardt**
Institute for Nano- and Microfluidics, Center of Smart Interfaces,
Techn. Univ. Darmstadt, Petersenstr. 17, 64287 Darmstadt, Germany
dietzel@csi.tu-darmstadt.de, hardt@csi.tu-darmstadt.de

KEY WORDS

Electrokinetics, streaming potential, Soret effect.

ABSTRACT

The effect of a linear temperature gradient transverse to the main flow direction of a pressure-driven symmetric electrolyte in a slit-microchannel is investigated, specifically with respect to the electrokinetic streaming potential. Under the assumption that the Soret effect is the same for each ion species, an analytical expression of the electric double layer (EDL) potential is derived based on the non-isothermal Nernst-Planck equations and the Poisson equation. For identical zeta potentials on both walls, the results indicate that the Soret effect compresses the EDL in the vicinity of the colder wall and expands it in the vicinity of the warmer wall. In case of a temperature-dependent electric permittivity, the generated asymmetry was found to be opposite to the one due to the Soret effect. In both cases, the EDL potential distribution becomes asymmetric with respect to the channel axis in comparison with isothermal conditions. It is found that the asymmetry of the EDL potential due to the Soret effect has a smaller influence on the streaming current than on the conduction current, which becomes proportional to the applied temperature difference δT. Consequently, the streaming potential decreases with increasing δT. The effect is more pronounced for larger values of the channel height h_0 scaled to the Debye thickness κ^{-1} but does not exceed 4% reduction within the parametric domain considered herein. The findings might be of relevance in novel electrokinetic thermal-to-electric energy converters where the electrokinetic streaming is driven thermally.

1. INTRODUCTION

Electrohydrodynamics and ion transport phenomena in conducting [1], weakly conducting, leaky dielectric [2] and dielectric fluids have received intense attention by the scientific community over the last couple of decades. This is owed to the rich variety of physical effects [3], in particular in conjunction with fluid-fluid and fluid-solid interfaces [4, 5] as well as non-uniformities of the bulk electric properties leading for instance to instabilities in channel flow [6] or to electro-convection [7]. The exploration of these phenomena led to an equally vast diversity of possible applications especially in the general framework of microfluidics, ranging from liquid pumping [8], electric field based fabrication methods [9, 10] to DNA-manipulation [11], to name a few. Ion transport in dilute electrolytes is commonly captured with the Nernst-Planck equation, while the Maxwell stresses added to the Navier-Stokes equation account for the momentum transfer between ions and the solvent. Being a manifestation of the Onsager reciprocal principle [12], this interaction gives rise to two distinct types of electrokinetic couplings with single-phase fluids: one where an electric field drives a fluid motion such as in electro-osmotic flow (EOF), and another where ions advected along with the fluid generate an electric field, described by the so-called streaming potential [13]. The latter is in the focus of this study. Electrokinetic phenomena are commonly tied to the excess of one ion species in the vicinity of an interfacial charge of opposite polarity, as for instance carried by submerged solid bodies or walls. The accumulated ions form the diffusion-dominated electric double

* Corresponding author

layer (EDL) which screens the surface charge. These ions remain mobile and are advected with the flow in electrokinetic streaming applications. The EDL is typically only a few to a couple of hundred nm thick, depending on the bulk ion concentration. The liquid outside the EDL is irrelevant for the advective ion streaming. However, it contributes to the counter-acting and usually undesired ion flux by means of electro-migration caused by the potential difference, i.e. the bulk conduction current. To minimize the detrimental influence of the bulk fluid, many studies on electrokinetics are therefore concerned with miniaturization strategies to obtain system dimensions of the same order as the EDL thickness [14, 15, 16]. In turn, the resulting increased surface-to-volume ratio promotes the importance of interfacial stresses such as in studies related to molecular and apparent slip at superhydrophic walls [17, 18] or free surface-guided electrokinetic channel flow [19]. These approaches aim to reduce viscous losses in areas of the fluidic domain where excess ion predominately accumulate, i.e. close to submerged bodies or walls carrying a surface charge. Most studies of the streaming potential are concerned with pressure-driven flow while comparatively few investigations were performed on shear-driven flow [20] or other sources of fluid propulsion in conjunction with electrokinetic effects: viscous stresses dominate micro-scale flows (Stokes-limit), and the governing equations become linear to leading order of the Reynolds number so that electrokinetic and fluid mechanical effects can be linearly superimposed; the streaming potential becomes a linear function of the driving pressure difference. For instance, in the general scope of energy sustainability efforts it is of interest to know whether the electrokinetic charge separation can be driven thermally [21] by using waste heat generated e.g. by the central processing unit (CPU) of a computer. However, most thermally induced fluid propulsion (buoyancy, thermocapillarity and Marangoni stresses, heat pipes) can be formulated -at least in the Stokes-limit- as an effective pressure difference which can be then combined with the conventional electrokinetic theory to estimate the streaming potential generated by a thermally propelled liquid. In this case, an integral study of thermal, fluid mechanical and electrokinetic effects appears to be not necessary. This holds as long as the temperature-field does not affect the distribution of the ions by means of thermal diffusion, i.e. the Soret-effect [22]. While the intrinsic Soret coefficient, the ratio between the thermal diffusion coefficient $D_{T,\mathrm{k}}$ of ion species k to the corresponding concentration-induced diffusion coefficient $D_{n,\mathrm{k}}$, is typically small for common electrolytes [23], it might still have a non-negligible effect in small-scale systems due to large temperature gradients.

This work accesses the implications and significance of thermally induced ion diffusion in symmetric electrolytes in non-isothermal electrokinetic charge separation processes. As a model system, a pressure-driven slit channel flow of a fully dissociated binary electrolyte subjected to a temperature gradient lateral to the channel axis is chosen. It is assumed that both ion species have the same temperature and concentration-induced diffusion coefficients. Taking advantage of the disparate ratio between channel height and channel length, the scaled non-isothermal Nernst-Planck equation leads to a second order, non-linear ordinary differential equation (ODE) of the EDL potential. This ODE is analytically solved in terms of modified Bessel functions, indicating that the distribution of the EDL potential is not according to the Boltzmann equation obtained under isothermal conditions but instead becomes asymmetric in lateral direction with respect to the channel center line. Assuming a parabolic velocity profile while neglecting the electro-osmotic contribution, the electrokinetic streaming potential is derived and compared to the one if the channel has a uniform temperature. In the following section II, an expression of the non-isothermal streaming potential depending on the axial pressure and lateral temperature difference, EDL thickness scaled to the slit height, surface zeta potential and Soret coefficient is derived. The streaming potential obtained is discussed for a realistic range of parameters in section III.

2. MODEL AND GOVERNING EQUATIONS

In the following, the governing equations are summarized and simplified to estimate the streaming potential obtained from a pressure driven flow inside a parallel-plate slit-microchannel subjected to a temperature gradient traverse to the main flow direction. The channel length is denoted by l_0, one half of the gap width is denoted by h_0. It is assumed that h_0 is much smaller than the axial extent l_0 and thus $A^2 = (h_0/l_0)^2 \ll 1$. The axial x-direction is scaled with l_0 while the lateral z-coordinate is scaled with h_0, i.e. $\vec{X} = (X, Z) = (x/l_0, z/h_0)$. The corresponding scaling velocities of the velocity vector $\vec{v} = (u, w)$ are u_0 and w_0, respectively, i.e. the non-dimensional velocity vector reads $\vec{V} = (U, W) = (u/u_0, w/w_0)$. The mass conservation equation for an incompressible fluid, $\nabla \cdot \vec{v} = 0$, reads in dimensionless form $\overline{\nabla} \cdot \vec{V} = 0$, where the non-dimensional Nabla-operator is $\overline{\nabla} = (\partial_X, \partial_Z)$ and $\partial_X \equiv \partial/\partial X$, $\partial_Z \equiv \partial/\partial Z$. This implies that $w_0 = Au_0$. The electrokinetic properties are commonly a strong function of the non-dimensional parameter κh_0, where $\kappa^{-1} =$

$\sqrt{\epsilon_{\text{liq}} k_{\text{B}} T_\infty/(2e^2\nu^2 n_\infty)}$ is the Debye-length of the electric double layer (EDL) near charged interfaces. The Boltzmann constant is denoted by k_{B}, and T_∞ is the ambient reference temperature. With ε_0 being the dielectric permittivity of vacuum and $\varepsilon_{\text{r,liq}}$ being the relative permittivity of the liquid, the (in general temperature-dependent) permittivity of the liquid is $\epsilon_{\text{liq}} = \varepsilon_0 \varepsilon_{\text{r,liq}} = f(T)$. The elementary charge is e, ν is the valence of the symmetric $\nu : \nu$ electrolyte, and n_∞ is the reference volumetric ion concentration far away from the walls.

2.1 Double-layer potential

Ion transport is governed by the Nernst-Planck-equations reading

$$d_t n_{\text{k}} = \nabla \cdot (D_{n,\text{k}} \nabla n_{\text{k}} + n_{\text{k}} D_{T,\text{k}} \nabla T + e\nu_{\text{k}} n_{\text{k}} \omega_{\text{k}} \nabla \psi), \tag{1}$$

where the substantial derivative is denoted by $d_t(.) = \partial_t(.) + \vec{v} \cdot \nabla(.)$ and $\partial_t \equiv \partial/\partial t$. The volumetric concentration of positive or negative ions labeled with $k = (+, -)$ is denoted by n_{k}, and T is the local absolute temperature. The diffusion coefficients due to concentration gradients are $D_{n,\text{k}}$, while $D_{T,\text{k}}$ are the temperature-induced diffusion coefficients of the ions subjected to an external temperature difference δT. The ion mobilities under the action of a gradient in the EDL potential, $\nabla\psi$, are denoted by $\omega_{\text{k}} \approx D_{n,\text{k}}/(k_{\text{B}} T)$. Assuming that the ion diffusion coefficients are constant it follows $d_t N_{\text{k}} = D_{n,\text{k}} \nabla \cdot (\nabla N_{\text{k}} + N_{\text{k}} S^*_{\text{k}} \delta T \nabla \Theta + \overline{\nu}_{\text{k}} N_{\text{k}} \nabla \Psi/[1 + \Theta \delta T/T_\infty])$ with $N_{\text{k}} = n_{\text{k}}/n_\infty$, $\Theta = (T - T_\infty)/\delta T$ and $\Psi = e\nu\psi/(k_{\text{B}} T_\infty)$. The intrinsic Soret coefficient of the ions is denoted by $S^*_{\text{k}} = D_{T,\text{k}}/D_{n,\text{k}}$ in units of K^{-1}, $\overline{\nu}_{\text{k}} = \nu_{\text{k}}/\nu$. With $d_\tau(.) \equiv \partial_\tau(.) + \vec{V} \cdot \overline{\nabla}(.) = (l_0/u_0) d_t(.)$, where $\tau = t u_0/l_0$ is the non-dimensional time scale, $\nabla = (A\partial_X, \partial_Z)/h_0$ and $\widetilde{\Theta} = 1 + \Theta \delta T/T_\infty$ one finds

$$\begin{aligned} A^2 \Bigg(\frac{l_0 u_0}{D_{n,\text{k}}} d_\tau N_{\text{k}} - \partial_X^2 N_{\text{k}} - N_{\text{k}} S^*_{\text{k}} \delta T \partial_X^2 \Theta - \frac{\overline{\nu}_{\text{k}} N_{\text{k}}}{\widetilde{\Theta}} \partial_X^2 \Psi \\ - S^*_{\text{k}} \delta T \partial_X N_{\text{k}} \partial_X \Theta - \frac{\overline{\nu}_{\text{k}}}{\widetilde{\Theta}} \partial_X N_{\text{k}} \partial_X \Psi + \frac{\overline{\nu}_{\text{k}} N_{\text{k}}}{\widetilde{\Theta}^2} \frac{\delta T}{T_\infty} \partial_X \Theta \partial_X \Psi \Bigg) = \\ \partial_Z^2 N_{\text{k}} + N_{\text{k}} S^*_{\text{k}} \delta T \partial_Z^2 \Theta + \frac{\overline{\nu}_{\text{k}} N_{\text{k}}}{\widetilde{\Theta}} \partial_Z^2 \Psi + S^*_{\text{k}} \delta T \partial_Z N_{\text{k}} \partial_Z \Theta + \frac{\overline{\nu}_{\text{k}}}{\widetilde{\Theta}} \partial_Z N_{\text{k}} \partial_Z \Psi - \frac{\overline{\nu}_{\text{k}} N_{\text{k}}}{\widetilde{\Theta}^2} \frac{\delta T}{T_\infty} \partial_Z \Theta \partial_Z \Psi \end{aligned} \tag{2}$$

For low to moderate temperature differences $\delta T \ll T_\infty$, it follows $\widetilde{\Theta} \approx 1$. For ionic solutions with $l_0 u_0/D_{n,\text{k}} \leq O(1)$ and $S^*_{\text{k}} \delta T \leq O(1)$ the left hand side (LHS) of Eq. (2) is then small at least to order A^2 and can be neglected. Neglecting also the last term in Eq. (2) (due to $\delta T/T_\infty \ll 1$), rearranging and integration in Z leads to $\partial_Z N_{\text{k}} + N_{\text{k}} \partial_Z \widetilde{\Psi}_{\text{k}} = c_1(X)$ where $\widetilde{\Psi}_{\text{k}} = \overline{\nu}_{\text{k}} \Psi + S^*_{\text{k}} \delta T \Theta$ and $c_1(X)$ is an integration constant. The latter is set to zero herein, assuming that the ion distribution does not change as a function of Z if no gradient in temperature or electric potential is present. Hence the local ion number density N_{k} follows the local potential $\widetilde{\Psi}_{\text{k}}$ in Z according to the Boltzmann distribution $N_{\text{k}} = c_2 \exp(-\widetilde{\Psi}_{\text{k}})$, where in case of non-isothermal conditions the electric potential needs simply to be corrected for the Soret effect. The integration constant c_2 is set to unity, i.e. all ion species have a uniform density n_∞ at $\widetilde{\Psi}_{\text{k}} = 0$. For a symmetric $\nu : \nu$-electrolyte with K species, the charge density ρ_{f} reads $\rho_{\text{f}}/(e\nu n_\infty) = \sum_{k=1}^{K} \overline{\nu}_{\text{k}} N_{\text{k}} = -\exp(-S^*_- \delta T \Theta)[\exp(\Psi) - \exp(-\delta S^* \delta T \Theta)\exp(-\Psi)]$ where $\delta S^* = S^*_+ - S^*_-$. For small differences in the intrinsic Soret coefficients of the anions and cations, $S^*_+ \approx S^*_- = S^*$ (i.e. a thermoelectric charge separation based on different mobilities of the charge carriers, equivalent to the Seebeck effect in solids, is absent) and small temperature differences δT, it follows $\exp(-\delta S^* \delta T \Theta) \approx 1$. In this case, the Soret effect only diminishes the local charge density by a factor of $f^2_{S^*} = \exp(-S^* \delta T \Theta)$. Then $\rho_{\text{f}}/(e\nu n_\infty) = -2 f^2_{S^*} \sinh(\Psi)$.

In non-dimensional form, the Poisson equation $\nabla \cdot (\epsilon \nabla \psi) = -\rho_{\text{f}}$ reads

$$A^2 \left(\partial_X^2 \Psi + \frac{\epsilon_T \delta T}{\epsilon_{\text{liq}}} \partial_X \Psi \partial_X \Theta \right) + \partial_Z^2 \Psi + \frac{\epsilon_T \delta T}{\epsilon_{\text{liq}}} \partial_Z \Psi \partial_Z \Theta = -\frac{1}{2} \overline{\kappa}^2 \sum_{k=1}^{K} \overline{\nu}_{\text{k}} N_{\text{k}}, \tag{3}$$

with $\overline{\kappa} = \kappa h_0$. The temperature dependence of the dielectric permittivity was incorporated with $\nabla \epsilon = \epsilon_T \nabla T$ where $\epsilon_T \equiv d\epsilon_{\text{liq}}/dT$. The terms with derivatives in axial direction are again small to order A^2 and can be neglected. The temperature distribution is governed by the energy equation. Neglecting viscous dissipation as well as the kinetic energy of the flow and assuming a constant thermal conductivity $k_{\text{liq,0}}$ of the electrolyte, this

is approximated by $dT/dt = \alpha_0 \nabla^2 T$. The thermal diffusivity is denoted by $\alpha_0 = k_{\text{liq},0}/(c_\text{p}\rho)$, where c_p is the heat capacity at constant pressure. In non-dimensional form, the energy equation reads

$$APe\,(d_\tau \Theta) - A^2 \frac{\partial^2 \Theta}{\partial X^2} = \frac{\partial^2 \Theta}{\partial Z^2} \tag{4}$$

where $Pe = h_0 u_0/\alpha_0$ is the Péclet number. For electrolytes with $Pe \leq O(A)$, the LHS can be neglected and it follows that the liquid temperature is a linear function, spanning the range between the lower wall temperature T_1 and the upper wall temperature T_2, i.e. $\Theta = Z$ ($\delta T = T_2 - T_1$) and $\partial_Z \Theta = 1$. With Eq. (3) and the common Debye-Hückel-approximation [$\Psi < 1 \rightarrow \sinh(\Psi) \approx \Psi$] this leads to

$$\partial_Z^2 \Psi + E^* \delta T \partial_Z \Psi - \overline{\kappa}^2 \exp(-S^* \delta T Z)\Psi = 0, \tag{5}$$

where $E^* = \epsilon_T/\epsilon_\text{liq}$. Focusing first on the effect of a temperature-dependent permittivity, the solution of Eq. (5) for $S^*\delta T = 0$ is

$$\Psi_{E^*\delta T} = \overline{\zeta}_{|\text{s}} \left[\frac{\exp(\overline{\kappa}_1 Z)}{\exp(\overline{\kappa}_1) - \exp(\overline{\kappa}_2)\frac{\sinh(\overline{\kappa}_1)}{\sinh(\overline{\kappa}_2)}} - \frac{\exp(\overline{\kappa}_2 Z)}{\exp(\overline{\kappa}_1)\frac{\sinh(\overline{\kappa}_2)}{\sinh(\overline{\kappa}_1)} - \exp(\overline{\kappa}_2)} \right], \tag{6}$$

where $\overline{\kappa}_{1/2} = E^*\delta T/2 \pm \sqrt{(E^*\delta T/2)^2 + \overline{\kappa}^2}$. A constant (non-dimensional) zeta potential $\overline{\zeta}_{|\text{s}} = e\nu\zeta_{|\text{s}}/(k_\text{B}T_\infty)$ was used at the walls ($Z = \pm 1$) with $\zeta_{|\text{s}}$ as the dimensional zeta-potential. For $\epsilon_T = 0$, $\overline{\kappa}_{1/2} \equiv \pm\overline{\kappa}$, and Eq. (6) reproduces the well-known symmetric EDL-potential distribution for a parallel-plate configuration, reading $\Psi_{\epsilon_T=0,S^*=0} = \overline{\zeta}_{|\text{s}}\cosh(\overline{\kappa}Z)/\cosh(\overline{\kappa})$. In Fig. 1 (a), the EDL potential relative to the zeta-potential, as expressed with Eq. (6), is plotted as a function of the lateral channel coordinate Z for $E^*\delta T = -0.5$ and $\overline{\kappa} = (0.5, 1, 5, 10)$. For illustrative purposes, the value of $E^*\delta T$ is chosen relatively high in this plot, considering that $E^* = -5{\cdot}10^{-2}\text{K}^{-1}$ for a 0.01 M NaCl electrolyte solution [24]. Note that $\Psi/\overline{\zeta}_{|\text{s}} = \psi/\zeta_{|\text{s}}$. Under the present assumption of identical zeta potentials on both channel walls and in comparison to isothermal conditions, the plot indicates that a temperature-dependent electric permittivity of an electrolyte, which is subjected to a linear temperature gradient, expands the EDL in vicinity of the colder wall and compresses the EDL in vicinity of the warmer wall. The EDL potential distribution becomes asymmetric. The effect is the largest for $\overline{\kappa} = 1$, i.e. when the channel half height is of the same order as the EDL thickness, and vanishes quickly for larger values of $\overline{\kappa}$. Exemplary for $\overline{\kappa} = 1$, the inset of this figure depicts the dependence of the EDL potential on the specific value of $E^*\delta T$.

On the other hand, neglecting the temperature-dependent permittivity but including the intrinsic Soret effect, the solution of Eq. (5) involves the Bessel-functions of the first and second kind at zeroth order, $J_{0,\xi(Z)} = J_{r0,\xi(Z)} + i \cdot J_{i0,\xi(Z)}$ and $Y_{0,\xi(Z)} = Y_{r0,\xi(Z)} + i \cdot Y_{i0,\xi(Z)}$, respectively. The 'r' in the subscript of each Bessel function refers to the real part and the 'i' to the imaginary part. For $E^*\delta T = 0$ this leads to

$$\Psi_{S^*\delta T} = \overline{\zeta}_{|\text{s}} \frac{[Y_{r0,\xi(Z=-1)} - Y_{r0,\xi(Z=1)}]J_{r0,\xi(Z)} - [J_{r0,\xi(Z=-1)} - J_{r0,\xi(Z=1)}]Y_{r0,\xi(Z)}}{J_{r0,\xi(Z=1)}Y_{r0,\xi(Z=-1)} - J_{r0,\xi(Z=-1)}Y_{r0,\xi(Z=1)}}, \tag{7}$$

where the (complex) argument of the Bessel functions is $\xi(Z) = 2i\overline{\kappa}/(S^*\delta T)\exp(-S^*\delta T Z/2)$. In Fig. 1 (b), the EDL potential distribution in Z, as expressed with Eq. (7) and accounting for the Soret-effect, is plotted for $S^*\delta T = 0.5$ and $\overline{\kappa} = (0.5, 1, 5, 10)$. To ease illustration, the chosen value for $S^*\delta T$ is again relatively high in comparison with typical values of the intrinsic Soret coefficient for a 0.01 M NaCl electrolyte, which are in the range of $O(10^{-3}) \leq S^* \leq O(10^{-2})$ [25, 26, 27]. In contrast to the case of a temperature-dependent electric permittivity, the Soret-effect compresses the EDL in the vicinity of the colder wall and expands it in the vicinity of the warmer one compared to isothermal conditions. The inset of this figure shows the dependence of the EDL potential on $E^*\delta T$ exemplary for $\overline{\kappa} = 1$. However, other than for a temperature-dependent electric permittivity, the effect does not vanish quickly for larger values of $\overline{\kappa}$.

In summary, the EDL of electrolytes in channels with equally charged walls and subjected to a linear temperature gradient is expanded either at the colder wall (temperature-dependent permittivity) or at the warmer wall (Soret-effect) compared to the isothermal case. The effect is reversed at the opposite wall, leading in both cases to an asymmetric distribution of the EDL potential in Z. In the following derivation of the streaming potential under the action of a temperature gradient traverse to the main flow direction, we focus our attention on the Soret-effect, since it should have a noticeable effect on the EDL-potential also at larger values of $\overline{\kappa}$.

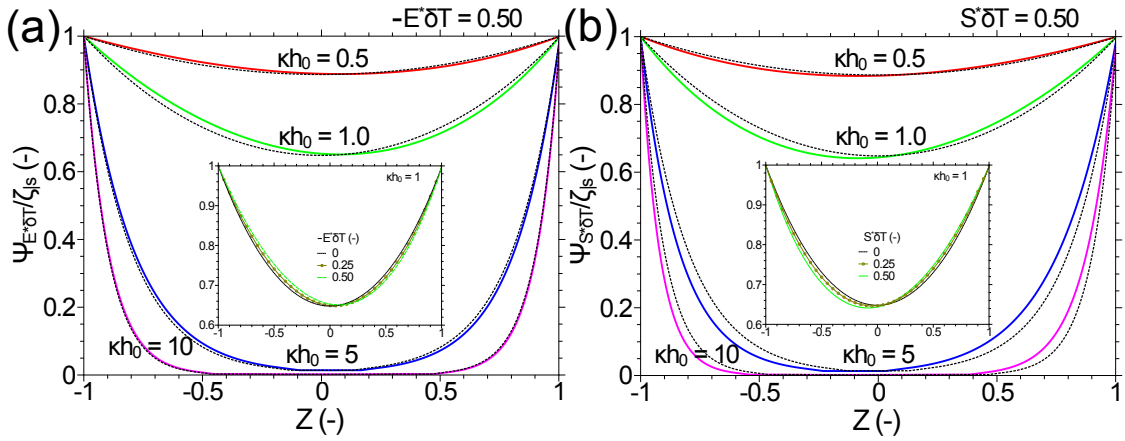

Figure 1: Ratio $\Psi/\overline{\zeta}_{|\mathrm{s}} = \psi/\zeta_{|\mathrm{s}}$ of the EDL potential relative to applied zeta potential as a function the lateral channel coordinate Z. (a) Effect of temperature-dependent electric permittivity. $\Psi = \Psi_{E^*\delta T}$ was calculated with Eq. (6). $\overline{\kappa} = (0.5, 1, 5, 10)$ at $-E^*\delta T = 0.5$ or $-E^*\delta T = (0, 0.25, 0.5)$ at $\overline{\kappa} = 1$ (inset). (b) Soret-effect. $\Psi = \Psi_{S^*\delta T}$ was calculated with Eq. (7). $\overline{\kappa} = (0.5, 1, 5, 10)$ at $S^*\delta T = 0.5$ or $S^*\delta T = (0, 0.25, 0.5)$ at $\overline{\kappa} = 1$ (inset). In all cases shown, the dotted black lines are the corresponding isothermal EDL-potential distributions.

2.2 Axial velocity profile

We assume that the pressure driven flow inside the channel is fully developed and unaffected by the streaming potential, i.e., as a first approximation, the flow field modification due to electro-osmosis is neglected. In this case, the non-dimensional axial velocity simply reads

$$U = -\frac{\partial_X P_0}{2}(1 - Z^2). \tag{8}$$

The axial, dimensionless pressure gradient is denoted by $\partial_X P_0$, where $P = Ah_0 p/(u_0\eta_0)$ with p as the original (dimensionful) pressure; η_0 is the dynamic viscosity. The average axial velocity of the parabolic profile is taken as the scaling velocity, i.e. $u_0 = \delta p_0 A h_0/(3\eta_0)$. The Reynolds-number is then $Re = A\rho\delta p_0 h_0^2/(3\eta_0^2)$ and the Péclet-number $Pe = A\delta p_0 h_0^2/(3\alpha_0\eta_0)$. The ratio between the transport by advection to the one by diffusion is $l_0 u_0/D_n = \delta p_0 h_0^2/(3D_n\eta_0)$.

2.3 Electric Currents and Streaming Potential

The total electric current due to ion motion driven by advection and by electro-migration vanishes at stationary conditions. This leads to a streaming electric field $\mathrm{E_{st}} = -\partial_X \Phi_{\mathrm{st}}$ in lateral direction. The total lateral streaming current is $I_{\mathrm{st,x}} = b\int_{-h_0}^{h_0} \rho_{\mathrm{f}} u dz$ with b as the plane width of the slit-micro-channel. Here, we focus our attention on the modification of the streaming potential due to the Soret effect, i.e. in the following we have $\epsilon_T = 0$ ($E^* = 0$). Considering that $\rho_{\mathrm{f}}/(e\nu n_\infty) = \sum_{k=1}^{K} \overline{\nu}_{\mathrm{k}} N_{\mathrm{k}}$, neglecting the $O(A^2)$-term in Eq. (3) and integrating by parts under the given boundary condition of no slip at the walls, one finds $I_{\mathrm{st,x}} = bu_0\epsilon k_{\mathrm{B}} T_\infty/(h_0 e\nu)\int_{-1}^{1} \partial_Z U \partial_Z \Psi dZ$. This can be reformulated with Eq. (8) to read

$$I_{\mathrm{st,x}} \frac{\nu e}{b\kappa u_0 \epsilon k_{\mathrm{B}} T_\infty} = \frac{\partial_X P_0}{\overline{\kappa}} \left(2\overline{\zeta}_{|\mathrm{s}} - \int_{-1}^{1} \Psi dZ \right) \tag{9}$$

The electro-migration current (conduction current) induced by the streaming potential reads $I_{\mathrm{df,x}} = -bD_n e^2 /(k_{\mathrm{B}} T_\infty)\partial_x \phi \int_{-h_0}^{h_0} \sum_{k=1}^{K} \nu_k^2 n_k dz$. As derived in section 2.1, we have $n_k/n_\infty = N_{\mathrm{k}} = \exp(-\widetilde{\Psi}_{\mathrm{k}})$. If the thermal diffusion coefficients are identical for each ion species, it follows that $\sum_{k=1}^{K} \nu_k^2 n_k = \nu n_\infty \exp(-S^*\delta T\Theta)$ $\cosh(\Psi)$. For small $\Psi < 1$ we have $\cosh(\Psi) \approx 1 + \Psi^2/2$, leading with $\Theta = Z$ to

$$I_{\mathrm{df,x}} \frac{\nu e}{b\kappa u_0 \epsilon k_{\mathrm{B}} T_\infty} = -\frac{D_n}{u_0 l_0} \overline{\kappa} \partial_X \Phi_{\mathrm{st}} \left[2\frac{\sinh(S^*\delta T)}{S^*\delta T} + \frac{1}{2}\int_{-1}^{1} \exp(-S^*\delta T Z)\Psi^2 dZ \right]. \tag{10}$$

The streaming potential is calculated by setting the total current, as the sum of the streaming current [Eq. (9)] and the conduction current [Eq. (10)], equal to zero. After reinserting the definitions of the dimensionless

parameters to obtain dimensional values, one finds for the streaming potential $\delta\phi_{\text{st}}$ per pressure difference δp_0

$$\frac{\delta\phi_{\text{st}}}{\delta p_0} = \frac{k_{\text{B}}T_\infty/(e\nu)}{\kappa^2 D_n \eta} \frac{\overline{\zeta}_{|\text{s}} - \frac{1}{2}\int_{-1}^{1}\Psi dZ}{\frac{\sinh(S^*\delta T)}{S^*\delta T} + \frac{1}{4}\int_{-1}^{1}\exp(-S^*\delta T Z)\Psi^2 dZ} \tag{11}$$

Equation (11) is a first order approximation in A as long as $A^2 \ll 1$, $\delta T/T_\infty \ll 1$, $l_0 u_0/D_{n,\text{k}} \leq O(1)$, $S^*_{\text{k}}\delta T \leq O(1)$, $Re \leq O(A)$ and $Pe \leq O(A)$. Electro-osmosis is neglected. For comparison, in an isothermal channel within the Debye-Hückel-approximation and neglecting the electro-osmotic contribution the streaming potential reads [28]:

$$\left(\frac{\delta\phi_{\text{st}}}{\delta p_0}\right)_{|S^*\delta T=0} = \frac{k_{\text{B}}T_\infty/(e\nu)}{\kappa^2 D_n \eta} \frac{\overline{\zeta}_{|\text{s}}\left[1 - \frac{\tanh(\overline{\kappa})}{\overline{\kappa}}\right]}{1 + \frac{1}{4}\overline{\zeta}^2_{|\text{s}}\left[\frac{\tanh(\overline{\kappa})}{\overline{\kappa}} + \frac{1}{\cosh^2(\overline{\kappa})}\right]} \tag{12}$$

3. RESULTS AND DISCUSSION

For $\overline{\kappa} \to 0$, the EDL potential can be expected to have a uniform value $\Psi \approx \overline{\zeta}_{|\text{s}}$, with little effect of thermal ion diffusion. In this case, one can deduce from Eq. (11) and Eq. (12) that the ratio of the non-isothermal/isothermal streaming potentials should attain the value of

$$\lim_{\overline{\kappa}\to 0} \frac{\delta\phi_{\text{st}}}{(\delta\phi_{\text{st}})_{\text{isoth}}} = \frac{S^*\delta T}{\sinh(S^*\delta T)} \tag{13}$$

On the other hand, for very large $\overline{\kappa}$, one might expect that the modification of the EDL-potential by the Soret-effect compared to isothermal conditions is insignificant since the EDL thickness is very small compared to the channel height. In this case, the EDL potential can be approximated with the isothermal expression, i.e. $\Psi \approx \overline{\zeta}_{|\text{s}}\cosh(\overline{\kappa}Z)/\cosh(\overline{\kappa})$. In the limit of $\overline{\kappa} \to \infty$, one finds

$$\lim_{\overline{\kappa}\to\infty} \frac{\delta\phi_{\text{st}}}{(\delta\phi_{\text{st}})_{\text{isoth}}} = \frac{1 + \frac{1}{2}\overline{\zeta}^2_{|\text{s}}}{\frac{\sinh(S^*\delta T)}{S^*\delta T} + \frac{1}{2}\overline{\zeta}^2_{|\text{s}}} \tag{14}$$

Apparently, ion diffusion due to a temperature gradient transverse to the main flow direction generally decreases the streaming potential. This can be reasoned with Eqs. (9) and (10): the streaming current is affected by the Soret effect only indirectly by the Soret-induced modification of the EDL potential. On the other hand, the conduction current becomes directly dependent on $S^*\delta T$, so that it increases with increasing Soret-coefficient, diminishing the streaming potential.

Figure 2 depicts the ratio $(\delta\phi_{\text{st}})/(\delta\phi_{\text{st}})_{\text{isoth}}$ of non-isothermal/isothermal streaming potentials for four values of the dimensionless Soret parameter, $S^*\delta T = (0.05, 0.25, 0.4, 0.5)$. Typical intrinsic Soret-coefficients of binary electrolytes range between $O(10^{-3}) \leq S^* \leq O(10^{-2})$ [25, 26, 27] and we assumed temperature differences between $25 \leq \delta T \leq 50$K. All other thermophysical properties relevant for this study are listed in Table 1. The streaming potential accounting for the Soret effect was computed from Eq. (11), numerically integrating the expression for the EDL potential [Eq. (7)]. The isothermal streaming potential was calculated with Eq. (12). The non-dimensional zeta-potential was kept at $\overline{\zeta}_{|\text{s}} = 1$, which is the upper limit where the Debye-Hückel-approximation is valid. The plots confirms that the Soret effect due to a temperature gradient transverse to the flow direction reduces the streaming potential. The effect is relatively weak and remains within 4% reduction witin the parametric range considered herein. By contrast to the asymptotic considerations made before, the effect is weaker for smaller values of $\overline{\kappa}$ than for larger ones but the ratio $(\delta\phi_{\text{st}})/(\delta\phi_{\text{st}})_{\text{isoth}}$ reaches indeed a constant value for $\overline{\kappa} > 10$. The relatively sharp decrease of the streaming ratio can be explained with a reduction of EDL overlap for increasing $\overline{\kappa}$. For $S^*\delta T = 0.05$, the ratio could only be evaluated up to $\overline{\kappa} = 16$. The EDL-potential is quasi-symmetric in this case. Within standard rounding accuracy, its computer-based evaluation with Eq. (7) was no longer possible.

4. CONCLUSIONS

In conclusion, we investigated the effect an intrinsic Soret-effect has on the pressure-driven electrokinetic ion streaming of a symmetric electrolyte confined in a narrow slit channel subjected to a linear thermal gradient

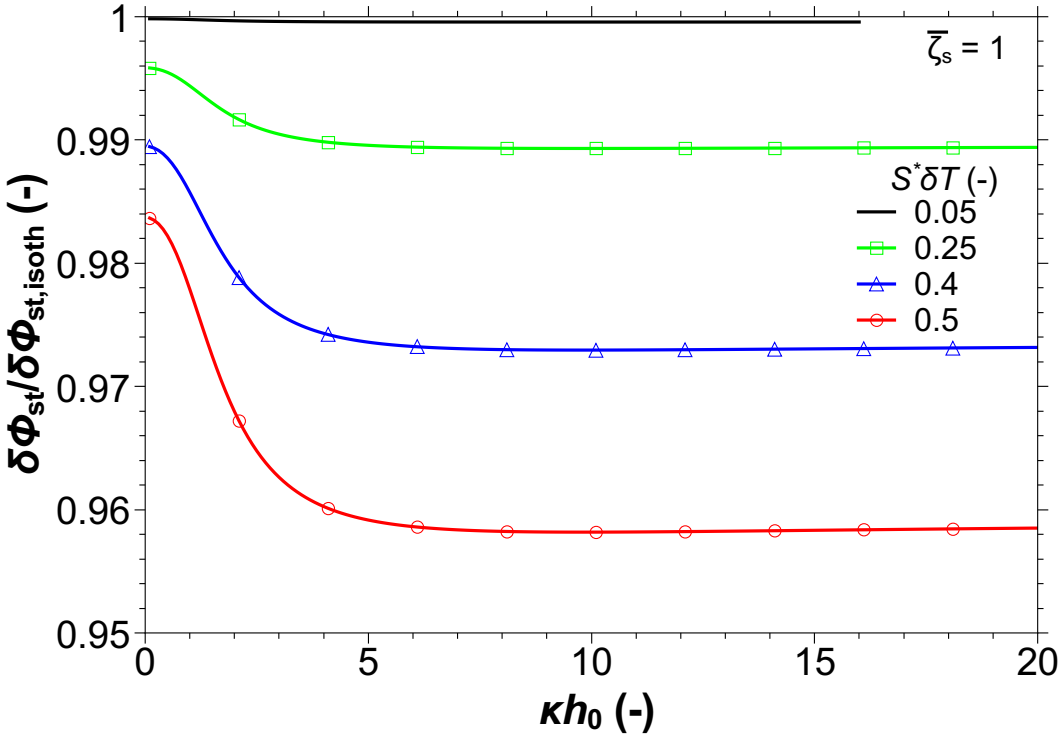

Figure 2: Ratio $(\delta\phi_{\text{st}})/(\delta\phi_{\text{st}})_{\text{isoth}}$ of non-isothermal/isothermal streaming potentials as a function of $\overline{\kappa} = \kappa h_0$ with $S^*\delta T$ as parameter and constant permittivity ($\epsilon_T = 0$). The streaming potential $\delta\phi_{\text{st}}$ was computed from Eq. (11) by numerical integration of Eq. (7). The isothermal streaming potential $(\delta\phi_{\text{st}})_{\text{isoth}}$ was calculated with Eq. (12). The non-dimensional zeta-potential was held constant at $\overline{\zeta}_{|\text{s}} = 1$ while the non-dimensional Soret-parameter varies from $0.05 \leq S^*\delta T \leq 0.5$.

.

$\rho_0(\text{kgm}^{-3})$	997 [29]	$\eta_0(m\text{Pa s})$	0.89 [29]	$\alpha_0(\text{m}^2\text{s}^{-1})$	$1.45 \cdot 10^{-7}$ [29]
$u_0(\text{ms}^{-1})$	$O(10^{-6}\text{-}10^{-2})$	Re (-)	$O(10^{-7}\text{-}10^{-1})$	Pe (-)	$O(10^{-6}\text{-}10^{-1})$
$h_0(\mu\text{m})$	≤ 2	$\zeta_{\|\text{s}}(\text{mV})$	≤ 25	$\delta T(\text{K})$	≤ 50
$\epsilon_{\text{liq}}/\varepsilon_0$ (-)	78.14 [24]	$\epsilon_T/\epsilon_{\text{liq}}(\text{K}^{-1})$	$-5 \cdot 10^{-2}$ [24]	$\kappa(\text{m}^{-1})$	$O(10^7)$
$D_n(\text{m}^2\text{s}^{-1})$	$O(10^{-9})$ [27]	$S^*(\text{K}^{-1})$	$O(10^{-3}\text{-}10^{-2})$ [25, 26, 27]	$l_0 u_0/D_n$ (-)	$O(10^{-3}\text{-}10^1)$

Table 1: Thermophysical properties and characteristic numbers. The solvent properties, listed in the first three rows of the table are based on pure water. The electric and transport properties of the solute, listed in the last two rows, refer to a 0.01 M NaCl-electrolyte solution. The corresponding values for a KCl-electrolyte are of the same order of magnitude. If not stated otherwise, all values were determined at 25^oC. The selected pressure differences are in the range of $1\text{Pa} \leq \delta p_0 \leq 10^2\text{Pa}$, and $A = 0.1$.

transverse to the flow direction. Within the validity of the slender-gap- and Debye-Hückel-approximation, the streaming potential is in general decreased by the Soret-effect, owing to the stronger dependence of the conduction current on the Soret-effect compared to the streaming current. The reduction is stronger for larger values of $\overline{\kappa}$ than for smaller values, and the ratio attains a constant value for values $\overline{\kappa} > 10$. Within the parametric domain considered, the streaming potential is decreased by not more than 4% compared to the isothermal case. It was shown that the Soret-effect but also a temperature-dependent electric permittivity leads to an asymmetric distribution of the double layer potential with respect to the channel mid plane. The Soret-effect compresses the EDL in the vicinity of the colder wall and expands it in the vicinity of the warmer, while the opposite occurs for a temperature-dependent permittivity. The latter affects the EDL only for very small values of $\overline{\kappa}$, while the Soret-effect remains in effect also for larger values. The findings are useful within the general scope of small-scale fluidic waste-exergy recovery units where the electrokinetic streaming is driven thermally.

ACKNOWLEDGEMENTS

M.D. acknowledges the fruitful discussion with Jeevanjyoti Chakraborty.

REFERENCES AND CITATIONS

[1] Taylor, G.I., & McEwan, A.D. (1965). The stability of a horizontal fluid interface in a vertical electric field. J. Fluid Mech.,22, 1-15
[2] Saville, D. A. (1997). Electrohydrodynamics: The Taylor-Melcher leaky dielectric model. Annu. Re. Fluid Mech., 29, 27-64.
[3] Castellanos, A. (1998). Electrohydrodynamics. Vienna: Springer.
[4] Melcher, J. R., & Taylor, G.I. (1969). Electrohydrodynamics: A review of the role of interfacial stresses. Annu. Rev. Fluid Mech., 1, 111-146.
[5] Pascall, A. J., & Squires, T. M. (2011). Electrokinetics at liquid/liquid interfaces. J. Fluid Mech., 684, 163-191.
[6] Lin, H., Storey, B. D., Oddy, M. H., Chen, C. H., & Santiago, J. G. (2004). Instability of electrokinetic microchannel flows with conductivity gradients. Phys. Fluids, 16, no. 6, 1922-1935
[7] Wong, J., & Melcher, J. R. (1969). Thermally induced electroconvection. Phys Fluids, 11, 2588.
[8] Ramos, A., González, A., Castellanos, A., Green, N. G., & Morgan, H. (2003). Pumping of liquids with ac voltages applied to asymmetric pairs of microelectrodes. Phys. Rev. E, 67, 056302
[9] Schäffer, E., Thurn-Albrechet, T., Russel, T.P., & Steiner, U. (2000). Electrically induced structure formation and pattern transfer. Nature, 403, 874-877.
[10] Galliker, P., Schneider, J., Eghlidi, H., Kress, S., Sandoghdar, V., & Poulikakos, D. (2012) Direct printing of nanostructures by electrostatic autofocussing of ink nanodroplets. Nat. Comm., 3:890
[11] Hahn, T., & Hardt, S. (2011). Concentration and size separation of DNA samples at liquid-liquid interfaces. Anal. Chem. 83, 5476-5479.
[12] Onsager, L. (1931). Reciprocal relations in irreversible processes I. Phys. Rev., 37, 405-426.
[13] Yang, J., Lu, F., Kostiuk, L. W., & Kwok, D. Y. (2003). Electrokinetic microchannel battery by means of electrokinetic and microfluidic phenomena. J. Micromech. Microeng., 13, 963-970.
[14] van der Heyden, F. H. J., Stein, D., & Dekker, C. (2005). Streaming currents in single nanofluidic channel. Phys. Rev. Lett., 95, 116104.
[15] Daguji, H. (2009). Ion transport in nanofluidic channels. Chem. Soc. Rev., 39, 901-911.
[16] Xie, Y., Sherwood, J. D., Shui, L., van den Berg, A., & Eijkel, J. C. T. (2011). Strong enhancement of streaming current power by application of two phase flow. Lab Chip, 11, 4006-4011.
[17] Yang, J., & Kwok, D. Y. (2004). Analytical treatment of electrokinetic microfluidics in hydrophobic microchannels. Analyt. Chim. Acta, 507, 39-53.
[18] Zhao, H. (2011). Streaming potential generated by a pressure-driven flow over superhydrophobic stripes. Phys. Fluids, 23, 022003.
[19] Lee, J. S. H., Barbulovic-Nad, I., Wu, Z., Xuan, X., & Li, D. (2006). Electrokinetic flow in a free surface-guided microchannel. J. Appl. Phys., 99, 054905.
[20] Soong, C. Y., & Wang, S. H. (2004). Analysis of rotation-driven electrokinetic flow in microscale gap regions of rotating disk system. J. Coll. Int. Sci., 269, 484-498.
[21] Grosu, F. P., & Bologa, M. K. (2010). Thermoelectrohydrodynamic methods of energy conversion. Surf. Eng. Appl. Electrochem., 46, no. 6, 582-588.
[22] Würger, A. (2010). Thermal non-equilibrium transport in colloids. Rep. Prog. Phys. 73, 126601.
[23] Snowdon, P. N., & Turner, J. C. R. (1960). The Soret effect in some 0.01 normal aqueous electrolytes. Trans. Faraday Soc., 56, no. 10, 1409-1418.
[24] Buchner, R., Hefter, G. T. & May, P. M. (1999). Dielectric relaxation of aqueous NaCl solutions. Phys. Chem. A, 103, no. 1, 1-9.
[25] Agar, J. N., & Turner, J. C. R. (1960). Thermal diffusion in solutions of electrolytes. Proc. R. Soc. Lond. A, 255, 307-330.
[26] Leaist, D. G. (1990). Soret coefficients of mixed electrolytes. J. Sol. Chem., 19, no. 1, 1-10.
[27] Takeyama, N., & Nakashima, K. (1983). Thermodynamics in thermal diffusion in aqueous ion solutions. J. Phys. Soc. Japan, 52, no. 8, 2699-2705.
[28] Masliyah, J. H., & Bhattacharjee, S. (2006). Electrokinetics and Colloid Transport Phenomena. Hoboken,

New Jersey: John Wiley & Sons.

[29] Lide, D.R. (2009). CRC Handbook of Chemistry and Physics. 89th edn. Boca Raton: CRC Publishing Company.